Vol. 9 | July 2015

www.lpr-journal.org

LASER & PHOTONICS REVIEWS

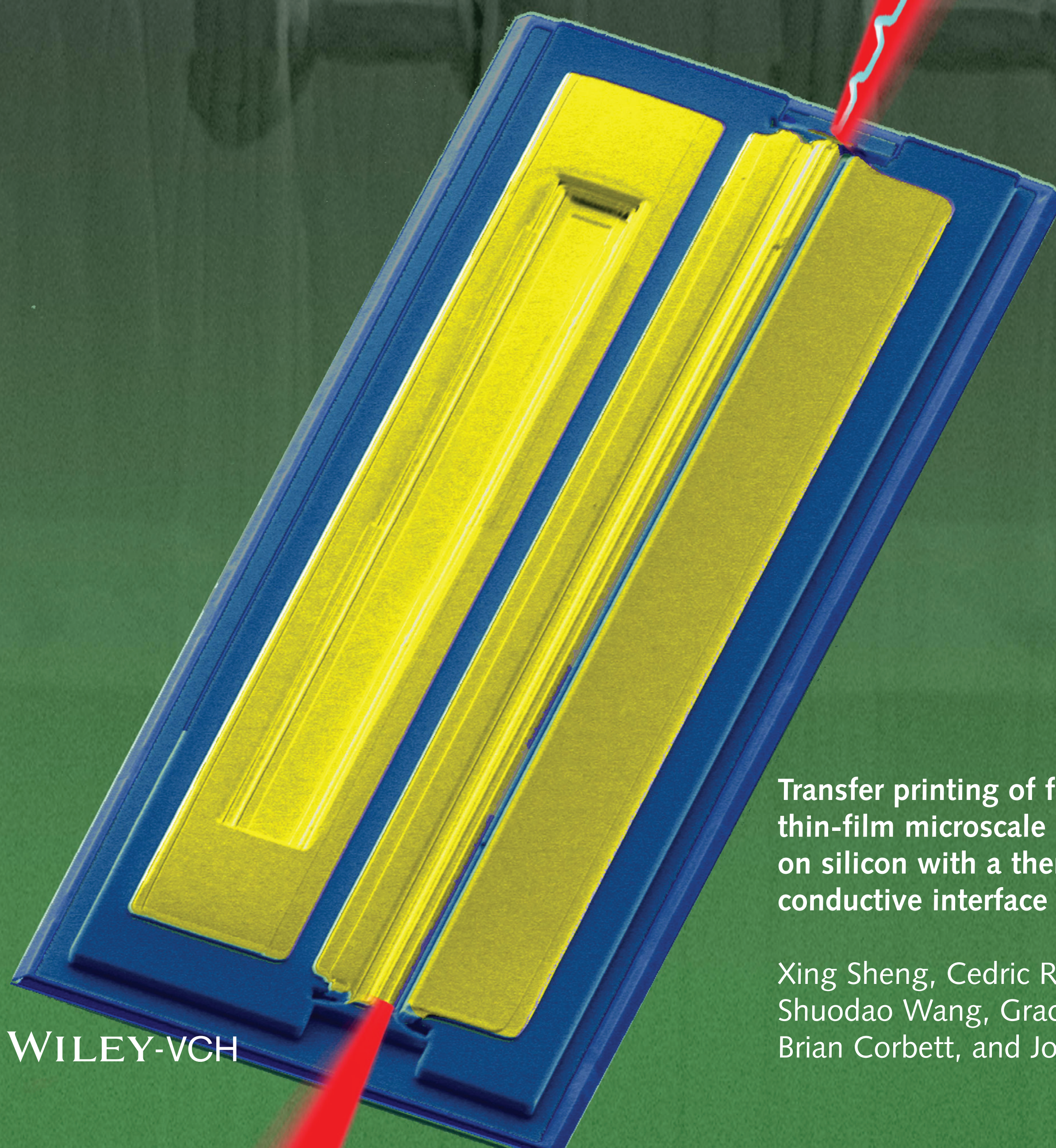

Transfer printing of fully formed thin-film microscale GaAs lasers on silicon with a thermally conductive interface material

Xing Sheng, Cedric Robert, Shuodao Wang, Grace Pakeltis, Brian Corbett, and John A. Rogers

WILEY-VCH

LASER
& PHOTONICS
REVIEWS

Laser Photonics Rev. **9,** No. 4, L17–L22 (2015) / **DOI** 10.1002/lpor.201500016

High performance semiconductor lasers on silicon are critical elements of next generation photonic integrated circuits. Transfer printing methods provide promising paths to achieve hybrid integration of III-V devices on Si platforms. This paper presents materials and procedures for epitaxially releasing thin-film microscale GaAs based lasers after their full fabrication on GaAs native substrates, and for subsequently transfer printing arrays of them onto Si wafers. An indium-silver based alloy serves as a thermally conductive bonding interface between the lasers and the Si, for enhanced performance. Numerical calculations provide comparative insights into thermal properties for devices with metallic, organic and semiconductor interfaces. Under current injection, the first of these three interfaces provides, by far, the lowest operating temperatures. Such devices exhibit continuous-wave lasing in the near-infrared range under electrical pumping, with performance comparable to unreleased devices on their native substrates.

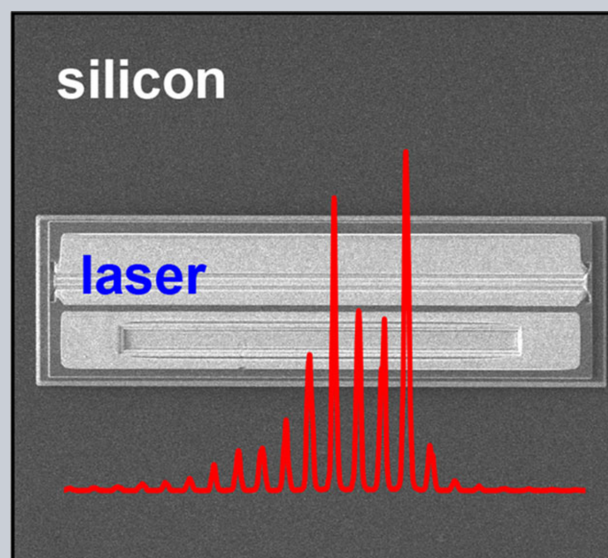

LETTER
ARTICLE

Transfer printing of fully formed thin-film microscale GaAs lasers on silicon with a thermally conductive interface material

Xing Sheng[1,], Cedric Robert[2,**], Shuodao Wang[3], Grace Pakeltis[1], Brian Corbett[2,*], and John A. Rogers[1,*]**

Silicon (Si) based complementary metal-oxide-semiconductor (CMOS) technology serves as the foundation for the entire integrated circuit (IC) industry. As Si CMOS approaches its scaling limits, interest increases in strategies capable of integrating alternative semiconductors and device structures on Si platforms [1]. For example, the potential for Si based photonics to improve performance (density, energy, speed, etc) in future IC chips [2–4] has created strong demand for efficient on-chip lasers [5]. Attempts to realize this goal range from use of Si Raman lasers to epitaxial growth of Ge or III-V compounds on Si [6–12]. In spite of much progress, such monolithic approaches do not yet provide the levels of performance that can be achieved in conventional III-V lasers. The challenges include low emission efficiencies in Si and Ge, and defects that arise from large lattice and thermal expansion coefficients mismatches between usual III-V materials (GaAs and InP) and Si and from the polar/non polar character of the III-V/Si interface [13]. By comparison, strategies that involve separate growth of III-V materials followed by integration on Si offer significant promise [14, 15]. Approaches based on epitaxial liftoff and transfer printing, in particular, have important proven capabilities in this context, with impressive published examples of both edge and surface emitting lasers formed with thin-film, releasable III-V membranes directly bonded to Si [16, 17]. In these schemes, selective removal by wet etching of an epitaxially grown sacrificial layer releases active material structures from the III-V substrate. Soft elastomer stamps serve as non-destructive tools to retrieve these materials and then to deliver them to Si wafers, in array formats in a single step or in a step and repeat fashion. This type of process offers high-speed operation and excellent overlay registration, enabled by controlled van der Waals bonding to the surface of the stamp. A disadvantage of previously reported work in active photonics is that it requires multi-step processing on the Si to complete the lasers, including definition of the cavity, contact metal deposition, etc. In addition, the

[1] Department of Materials Science and Engineering and Frederick Seitz Materials Research Laboratory, University of Illinois at Urbana-Champaign, Urbana, IL, 61801, USA
[2] Tyndall National Institute, University College Cork, Lee Maltings, Cork, Ireland
[3] Mechanical and Aerospace Engineering, Oklahoma State University, Stillwater, OK 74078, USA
** Authors contributed equally to this work
* Corresponding authors: e-mail: brian.corbett@tyndall.ie; jrogers@illinois.edu

© 2015 by WILEY-VCH Verlag GmbH & Co. KGaA, Weinheim

bonding between III-V materials and Si is most effective with atomically smooth surfaces, thereby creating high levels of sensitivity to parasitic roughness and defects. This paper presents concepts that bypass these challenges, and demonstrates them in strategies for releasing and transfer printing fully formed, functional thin-film microscale gallium arsenide (GaAs) based lasers onto Si substrates where a metallic thin film serves as an adhesive and a thermally conductive interface. Numerical simulations reveal the key considerations in thermal management, with an emphasis on the role of this interface layer. Electrically pumped devices printed on Si exhibit continuous-wave (CW) lasing in the near-infrared range (around 820 nm), with performance comparable to unreleased devices on their native substrates.

As schematically illustrated in Figure 1a, the device structure used here involves a GaAs based Fabry-Perot (etched facets) ridge waveguide laser, including two AlInGaAs quantum wells in the active gain region. The epitaxial structure includes a 1 μm thick $Al_{0.95}Ga_{0.05}As$ layer between the laser layers and the GaAs substrate, which serves as a sacrificial layer that can be removed by wet etching, as described subsequently. Unlike previous work [16], complete fabrication of the laser structure occurs on the GaAs substrate, using a standard sequence of steps in photolithography, etching, metal deposition and annealing (see Experimental section). A layer of silicon nitride (SiN_x, 470 nm thick) acts as a cladding layer to passivate the etched sidewalls and facets. The fabricated laser devices can be directly tested on the GaAs substrate, in an unreleased form. A layer of photoresist (~3 μm thick) patterned on the devices after eliminating the sacrificial layer in the exposed regions but before complete undercut serves as an additional protective coating on the laser sidewalls and front surfaces. After complete undercut, these photoresist structures (i.e. anchors) also hold the released devices in suspended forms at their original locations. The $Al_{0.95}Ga_{0.05}As$ sacrificial layer can be removed by hydrofluoric acid (HF) or hydrochloric acid (HCl) [18, 19]. Although HF etching is fast and can be applied in epitaxial liftoff for various GaAs and InGaP based device applications [20–22], HCl etching is preferred here due to its compatibility with various other materials in the laser structure such as the SiN_x cladding and the titanium-based contacts [23]. After HCl undercut, fully released lasers, along with the photoresist anchors, can be retrieved onto the surfaces of polydimethylsiloxane (PDMS) stamps (Figure 1b), individually or simultaneously as arrays. Delivery of devices to substrates of interest can occur in various adhesive-based and adhesiveless approaches [24]. Adhesiveless printing is attractive for its simplicity, but it demands extremely smooth and defect-free surfaces on the bottom sides of the lasers [16, 17, 23]. Organic adhesives relax such considerations [20–22] but they can impede heat dissipation due to their low thermal conductivities, thereby significantly degrading the laser performance, as discussed subsequently. In work presented here, a metallic based interface layer, analogous to those used in eutectic die bonding [25], facilitates heat transfer while maintaining high tolerance to surface roughness and defects, as illustrated in Figure 1c. Specifically, a commercially available eutectic

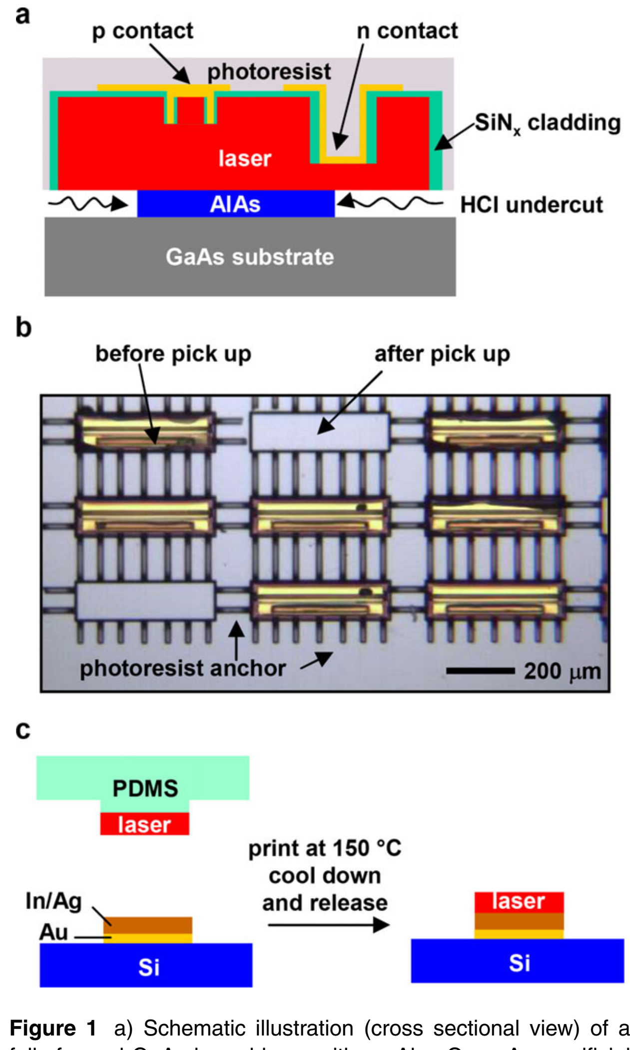

Figure 1 a) Schematic illustration (cross sectional view) of a fully formed GaAs based laser with an $Al_{0.95}Ga_{0.05}As$ sacrificial layer that can be etched selectively using HCl. b) Optical micrograph (top view) of an array of lasers tethered to the GaAs growth substrate. The $Al_{0.95}Ga_{0.05}As$ sacrificial layer has been removed, and some laser devices have been retrieved onto the surface of a PDMS stamp. c) Schematic illustration of a laser retrieved by a PDMS stamp and printed onto a Si substrate coated with an In/Ag alloy based paste layer.

indium-silver (97% In / 3% Ag) paste (Indalloy290, by Indium Corp.) is dispensed through a pneumatically operated syringe system, in which the final layer thickness is roughly controlled by the mass of the applied paste. (Industrial automated dispensing systems are available for automated application of such pastes [26]). More accurate layer thickness control can be achieved by evaporation or sputtering based metallization process [27]. Prior to application, the Si substrate is patterned with a thin-film gold (Au 100 nm) wetting layer that forms an intermetallic bond during reflow. Transfer printing occurs at the eutectic point of the In/Ag alloy (~150 °C), to allow reflow in the paste without affecting the any constituent materials in the laser structure. Removing the stamp after cooling to room temperature, and

© 2015 by WILEY-VCH Verlag GmbH & Co. KGaA, Weinheim

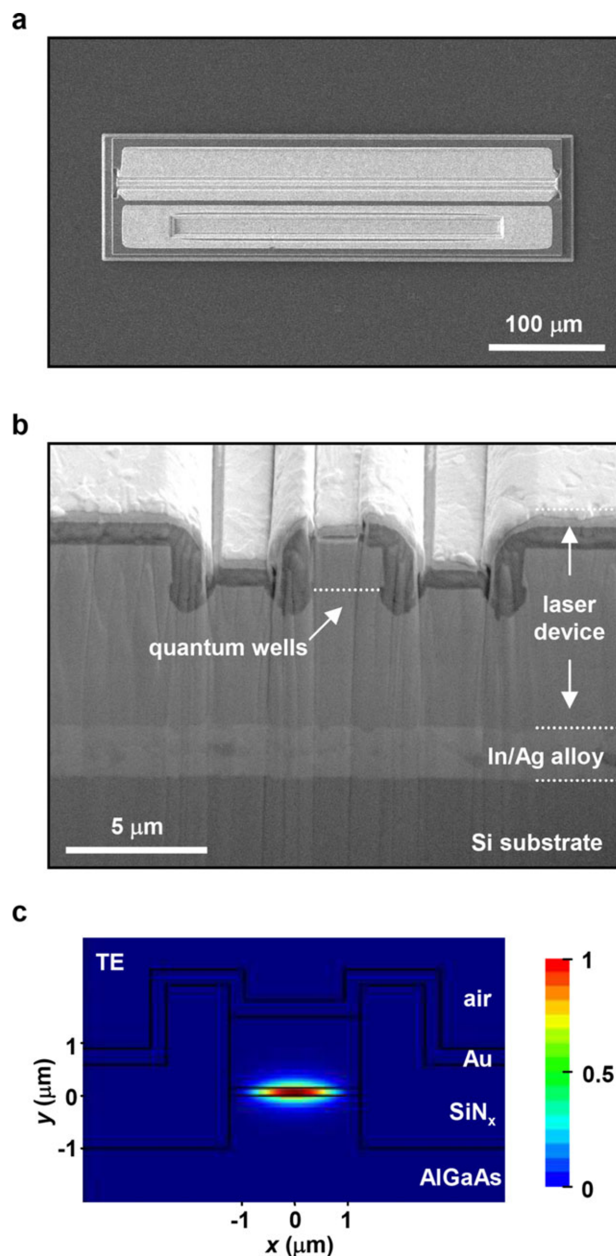

Figure 2 a) Top view and b) Cross sectional view SEM images of a laser printed on a Si substrate with an In/Ag alloy interface. c) Calculated electric field intensity $|\boldsymbol{E}|^2$ profile of the fundamental TE mode (at 820 nm) for the laser ridge waveguide structure.

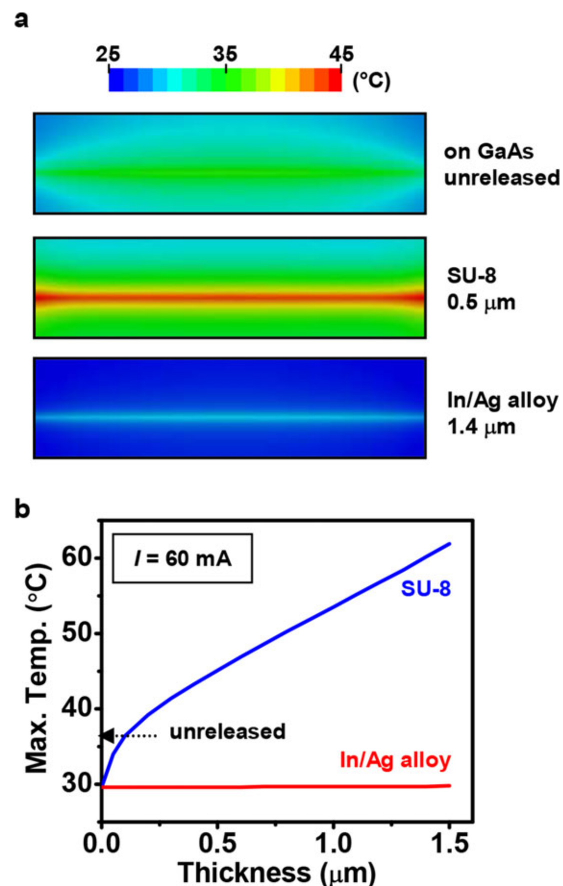

Figure 3 a) Calculated temperature distributions (top view) for lasers on different substrates with different interfaces at an injected electric power of 2.5 V × 60 mA = 0.15 W. The background temperature is set to 20 °C. The simulation map size is 400 μm × 100 μm. b) Calculated maximum temperatures reached on the front surfaces for lasers on Si, as a function of the interface layer (SU-8 and In/Ag) thickness. The data for the unreleased laser on GaAs is also indicated.

then eliminating the photoresist from the lasers by exposure to oxygen plasma etch completes the process.

Figure 2a presents a top view scanning electron microscope (SEM) micrograph of a laser printed on Si with a metallic In/Ag bonding interface. The device has an area of 400 μm × 100 μm, and a thickness of 5.8 μm. The cross sectional SEM image in Figure 2b illustrates the ridge waveguide structure as well as the In/Ag interface layer between the laser and Si. The waveguide has dimensions of 380 μm × 2.5 μm × 1.5 μm, protected by a SiN_x cladding layer with metallic contacts on top. The cavity length is thus 20 μm smaller than the total length of the device to include a recess of 10 μm on each facet. Devices with smaller recesses (5 μm and 0 μm) showed similar performance. The In/Ag interface layer has a thickness of ~1.4 μm. In such a waveguide laser with compressively strained AlInGaAs quantum wells, the gain for the transverse electric (TE) polarization is much larger than that of the transverse magnetic (TM) polarization, due to the strain induced splitting of the heavy/light hole bands [28]. Therefore, light emission is predominantly TE polarized. Figure 2c plots the calculated electric field intensity $|\boldsymbol{E}|^2$ profile of the fundamental TE mode at the wavelength of 820 nm, illustrating expected confinement of the optical mode to the quantum well gain region.

Figure 3 shows calculated results that predict the thermal performance for devices with different interface configurations. The model assumes that the injected CW electrical power (2.5 V × 60 mA = 0.15 W) fully converts

© 2015 by WILEY-VCH Verlag GmbH & Co. KGaA, Weinheim

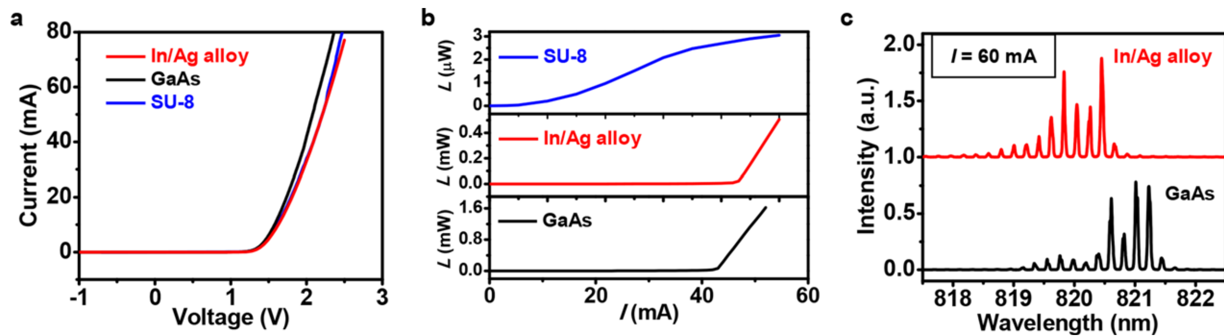

Figure 4 Performance for lasers on different substrates with different interfaces (unreleased on GaAs, on Si coated with 0.5 μm SU-8, on Si coated with 1.4 μm In/Ag). a) Current-voltage characteristics. b) Measured output light power *L* as a function of current *I* under CW operation. c) Emission spectrum of the lasers printed on Si with an In/Ag interface and on native GaAs substrates measured above threshold current ($I = 60$ mA). The emission peak linewidths are around 0.05 nm.

to thermal power homogeneously concentrated in the ridge waveguide region. Figure 3a plots steady-state temperature distributions on the device surface (top view) for lasers experimentally explored. The data indicate that the laser printed on Si with a 1.4 μm thick In/Ag interface exhibits a temperature that is lower even than that of the unreleased device on GaAs, due to the comparatively high thermal conductivity of In/Ag and of Si (82 W/K/m for In/Ag and 150 W/K/m for Si versus 55 W/K/m for GaAs). The laser printed on Si with a 0.5 μm thick SU-8 layer (conductivity 0.2 W/K/m) shows the highest temperature, consistent with its poor performance under CW operation. The maximum temperatures associated with the devices on GaAs, In/Ag, and SU-8 are 36.3 °C, 29.7 °C and 45.1 °C, respectively. Figure 3b further plots the calculated maximum temperatures on the laser surfaces as a function of the interface thickness. For the laser printed on the In/Ag interface, the device temperature is largely independent of the interface thickness and remains close to room temperature, due to the high thermal conductivity of the In/Ag alloy. For the laser printed on the SU-8 interface, the temperature depends strongly on the interlayer thickness. The calculations suggest that the temperature can be reduced to values comparable to those of the unreleased laser on GaAs when the SU-8 thickness is below 0.1 μm.

Figure 4 summarizes operating characteristics for lasers on different substrates. The current-voltage behavior on Si with the In/Ag interface corresponds to a typical GaAs diode response, as shown in Figure 4a. Similar results are obtained for devices on the native GaAs substrates as well as for devices printed on Si with organic based adhesives. Figure 4b presents the measured output light power from the etched laser facets, as a function of injected current under continuous-wave (CW) operation. At room temperature (~20 °C), the device printed on Si with the In/Ag interface exhibits a lasing threshold of ~43 mA (red curve), which is very similar to the an otherwise similar, unreleased device on GaAs (black curve). The light power is also similar between both devices (in the mW range per facet above the threshold). It is noted that the coupling between the lasers and the receiving photodiode is not optimized (see experimental section), so that the measured power may be significantly underestimated. Moreover, the coupling differs from one device to another, which may explain the differences between the measured power on the GaAs substrate and the one on the In/Ag coated Si substrate. As a comparison, the device printed on Si with a 0.5 mm thick organic (SU-8 polymer) based adhesive layer does not lase even at a very high injection current level (~100 mA) in CW mode and only exhibits spontaneous emission in the μW range per facet. Lasing can only be observed under a pulsed current operation. These results suggest that the thermal properties at the interfaces can have significant effects on lasing operation. Figure 4c illustrates emission spectra from the laser on Si with the In/Ag interface and the unreleased laser on native GaAs substrates at a current of 60 mA. The emission wavelengths are centered around 820 nm identically to the spectrum of the unreleased device (indicating no thermal degradation).

In summary, the results reported here demonstrate the possibilities for integrating fully formed thin-film microscale GaAs lasers on Si substrates using epitaxial release and transfer printing. This process has attributes that are well matched to use in scaled manufacturing, i.e. high throughput, parallel operation, high yields, excellent overlay registration, and is already in commercial use in the production of high concentration photovoltaic modules using automated high-speed printers [23]. The type of metallic interface introduced in here provides a highly thermally conductive bonding layer, thereby allowing device integration on patterned, non-planar Si IC chips in a back-end process, as well as onto other substrates like ceramics and polymers. Other advantages of the metallic interface include high electrical conductivity and optical reflectivity, which may provide future possibilities for advanced device design. One can envisage the integration of these transferred GaAs based lasers with post transfer deposited dielectric (SiO_2, SiN_x or polymer) waveguides via butt coupling strategies for example [14, 29, 30]. Furthermore, the printing and thermal management technologies are immediately applicable to InGaAsP and AlGaInAs lasers grown on InP substrates operating in the telecommunication band

© 2015 by WILEY-VCH Verlag GmbH & Co. KGaA, Weinheim

(wavelengths around 1.3 μm and 1.55 μm), which are highly temperature dependent [31]. These lasers can be made in a similar manner: InP etched facet lasers have been demonstrated previously [32], and InGaAs selective wet etching can be used for releasing the devices from the InP substrates [17,31]. The results presented here have promise as generalized routes for advanced heterogeneous integration in next-generation electronic and photonic circuits.

Experimental Section

Laser device fabrication: The GaAs based laser device structure was grown on a GaAs substrate using metal-organic chemical vapor deposition (MOCVD) (by IQE Inc.). The structure has a thickness of 5.7 μm, with two compressively strained AlInGaAs quantum wells [16]. A 1 μm thick $Al_{0.95}Ga_{0.05}As$ layer serves as a sacrificial layer between the active device and the GaAs substrate. The ridge waveguide and the trench for the n-contact were lithographically defined by BCl_3/Ar dry etching through a PECVD SiO_2 mask. The facets were lithographically defined by $SiCl_4$/He dry etching through a sputtered SiO_2 mask. Exposed sidewalls and facets were covered by 470 nm SiN_x. Ti/Au and Au/Ge/Au/Ni/Au were deposited as contacts for p-type and n-type GaAs, respectively, followed by larger Cr/Au bond pads. The fabricated waveguide ridge has a width of 2.5 μm, a depth of 1.5 μm, and a length of 380 μm. The laser size is 400 μm × 100 μm.

Laser device undercut and transfer printing: A photoresist layer (SPR220 v3.0) was patterned as an anchor layer to secure the fabricated layer device and protect the device surface during undercut. The sacrificial $Al_{0.95}Ga_{0.05}As$ layer was completely removed by immersing the wafer into a hydrochloric acid (HCl) solution (25% HCl in water) for 4 hours. Subsequently, individual released laser devices could be retrieved and printed onto Si based substrates by transfer printing with poly(dimethylsiloxane) (PDMS) stamps [24]. Prior to transfer, an In/Ag based paste layer (97% In + 3% Ag, Indalloy290, by Indium Corp.) was applied on Cr/Au (5 nm / 100 nm) coated Si substrates by drop casting. The printing process was performed at the eutectic point of the In/Ag alloy (~150 °C). After printing, the photoresist layer on the devices was removed by oxygen plasma etching.

Laser device characterization: The current-voltage curves of lasers were measured by a Keithley 2400 source meter at dark. The output light power vs. current curves were measured by collecting the light on a large area silicon photodiode (Newport 818 SL). Nevertheless, because we cannot put the photodiode closer than a few centimeters from the etched facet on our experimental setup, a significant part of the light is lost by reflection on the substrate before reaching the photodiode. These losses are more important for the devices printed on Si substrates (with In/Ag alloy and SU-8) than for the unreleased devices on GaAs substrate because the tested devices on Si are printed at the center of a few centimeter square Si piece whereas the tested devices on GaAs are very close to the edge of the GaAs piece. The laser emission spectra were obtained by collecting the light with a large numerical aperture optical fiber and dispersing it with an optical spectrum analyzer (Ando AQ6317B). Here again the coupling between the lasers and the fiber was not optimized. As a result, the light intensity plotted in Figure 4c is given in arbitrary units.

Optical and thermal modeling: In the optical simulation, the fundamental TE mode of the ridge waveguide was calculated at the wavelength of 820 nm, based on a finite difference algorithm (Lumerical Solutions, Inc.). The simulated layout was based on the cross sectional SEM structure (Figure 2b). The active quantum well core layers have a total thickness of 0.15 μm and an index of 3.52, sandwiched by $Al_{0.4}Ga_{0.6}As$ (index 3.38). The SiN_x cladding layer has an index of 2.0. In the thermal simulation, a 3D steady-state conjunct heat transfer finite element analysis model (ABAQUS Analysis) was used. The simulated device was assumed to be a GaAs block (400 μm × 100 μm × 6 μm). The injected electric power was assumed to be 2.5 V × 60 mA = 0.15 W, homogeneously concentrated in the waveguide region (400 μm × 2.5 μm × 6 μm). The thermal conductivities for GaAs, Si, In/Ag alloy and SU-8 are 55 W/K/m, 150 W/K/m, 82 W/K/m and 0.2 W/K/m, respectively.

Acknowledgements. This work was supported by Intel Corporation. C. Robert and B. Corbett also acknowledge Science Foundation Ireland under the Irish Photonic Integration Centre (IPIC) award 12/RC/2276.

Received: 16 January 2015, **Revised:** 8 April 2015,
Accepted: 8 May 2015

Published online: 1 June 2015

Key words: silicon photonics, GaAs lasers, transfer printing, electrical pumping, thermal management.

References

[1] International Technology Roadmap for Semiconductors. http://www.itrs.net, accessed: January, 2015.
[2] D. A. B. Miller, Proc. IEEE **97**, 1166 (2009).
[3] R. Kirchain and L. C. Kimerling, Nat. Photonics **1**, 303 (2007).
[4] A. Rickman, Nat. Photonics **8**, 579 (2014).
[5] D. Liang and J. E. Bowers, Nat. Photonics **4**, 511 (2010).
[6] H. Rong, R. Jones, A. Liu, O. Cohen, D. Hak, A. Fang, and M. Paniccia, Nature **433**, 725 (2005).
[7] J. Liu, X. Sun, R. Camacho-Aguilera, L. C. Kimerling, and J. Michel, Opt. Lett. **35**, 679 (2010).
[8] R. E. Camacho-Aguilera, Y. Cai, N. Patel, J. T. Bessette, M. Romagnoli, L. C. Kimerling, and J. Michel, Opt. Exp. **20**, 11316 (2012).
[9] M. E. Groenert, C. W. Leitz, A. J. Pitera, V. Yang, H. Lee, R. J. Ram, and E. A. Fitzgerald, J. Appl. Phys. **93**, 362 (2001).
[10] A. Lee, Q. Jiang, M. Tang, A. Seeds, and H. Liu, Opt. Exp. **20**, 22181 (2012).
[11] J. R. Reboul, L. Cerutti, J. B. Rodriguez, P. Grech, and E. Tournie, Appl. Phys. Lett. **99**, 121113 (2011).

© 2015 by WILEY-VCH Verlag GmbH & Co. KGaA, Weinheim

[12] S. Liebich, M. Zimprich, A. Beyer, C. Lange, D. J. Franzbach, S. Chatterjee, N. Hossain, S. J. Sweeney, K. Volz, B. Kunert, and W. Stolz, Appl. Phys. Lett. **99**, 071109 (2011).
[13] H. Kawanami, Sol. Energ. Mat. Sol. Cell **66**, 479 (2001).
[14] M. Lamponi, S. Keyvaninia, C. Jany, F. Poingt, F. Lelarge, G. de Valicourt, G. Roelkens, D. Van Thourhout, S. Messaoudene, J. M. Fedeli, and G. H. Duan, IEEE Photon. Tech. Lett. **24**, 76 (2012).
[15] A. W. Fang, H. Park, O. Cohen, R. Jones, M. J. Paniccia, and J. E. Bowers, Opt. Exp. **14**, 9203 (2006).
[16] J. Justice, C. Bower, M. Meitl, M. B. Mooney, M. A. Gubbins, and B. Corbett, Nat. Photonics **6**, 610 (2012).
[17] H. Yang, D. Zhao, S. Chuwongin, J. H. Seo, W. Yang, Y. Shuai, J. Berggren, M. Hammar, Z. Ma, and W. Zhou, Nat. Photonics **6**, 615 (2012).
[18] W. P. Dumke, J. M. Woodall, and V. L. Rideout, Solid-State Electron. **15**, 1339 (1972).
[19] P. Kumar, S. Kanakaraju, and D. L. Devoe, Appl. Phys. A. **88**, 711 (2007).
[20] J. Yoon, S. Jo, I. S. Chun, I. Jung, H. Kim, M. Meitl, E. Menard, X. Li, J. J. Coleman, U. Paik, and J. A. Rogers, Nature **465**, 329 (2010).
[21] X. Sheng, L. Shen, T. Kim, L. Li, X. Wang, R. Dowdy, P. Froeter, K. Shigeta, X. Li, R. G. Nuzzo, N. C Giebink, and J. A. Rogers, Adv. Energy Mater. **3**, 991 (2013).
[22] X. Sheng, C. J. Corcoran, J. He, L. Shen, S. Kim, J. Park, R. G. Nuzzo, and J. A. Rogers, Phys. Chem. Chem. Phys. **15**, 20434 (2013).
[23] X. Sheng, C. A. Bower, S. Bonafede, J. W. Wilson, B. Fisher, M. Meitl, H. Yuen, S. Wang, L. Shen, A. R. Banks, C. J. Corcoran, R. G. Nuzzo, S. Burroughs, and J. A. Rogers, Nat. Mater. **13**, 593 (2014).
[24] A. Carlson, A. M. Bowen, Y. Huang, R. G. Nuzzo, and J. A. Rogers, Adv. Mater. **24**, 5284 (2012).
[25] H. H. Hu, A. Bibl, J. A. Higginson, and H. F. S. Law, US008518204B2, (2013).
[26] EFD Inc., Air Powered Dispensing, http://www.nordson.com/en-us/divisions/efd/Literature/White-Papers/Solder/Nordson-EFD-Air-Powered-Dispensing.pdf, accessed: January, 2015.
[27] T. Kim, Y. H. Jung, J. Song, D. Kim, Y. Li, H. Kim, I. Song, J. J. Wierer, H. A. Pao, Y. Huang, and J. A. Rogers, Small **8**, 1643 (2012).
[28] S. L. Chuang, Physics of Optoelectronic Devices, (John Wiley & Sons, Inc., New York, NY, USA 1995).
[29] J. H. Lee, I. Shubin, J. Yao, J. Bickford, Y. Luo, S. Lin, S. S. Djordjevic, H. D. Thacker, J. E. Cunningham, K. Raj, X. Zheng, and A. V. Krishnamoorthy, Opt. Express **22**, 7678 (2014).
[30] R. Tseng, J. O'Callaghan, F. Eid, M. Gleeson, B. Rawlings, M. Kobrinsky, I. Ban, R. Nagle, W. McFarlane, B. Corbett, and P. Chang, Proc. OFC Th2A.41 (2014).
[31] H. H. Chang, A. W. Fang, M. N. Sysak, H. Park, R. Jones, O. Cohen, O. Raday, M. J. Paniccia, and J. E. Bowers, Opt. Express **15**, 11466 (2007).
[32] S. Dzioba, S. Jatar, T. V. Herak, J. P. D. Cook, J. Marks, T. Jones, and F. R. Shephard, Appl. Phys. Lett. **62**, 2486 (1993).

© 2015 by WILEY-VCH Verlag GmbH & Co. KGaA, Weinheim